Inorganic Chemistry Communications 127 (2021) 108546

Contents lists available at ScienceDirect

Inorganic Chemistry Communications

journal homepage: www.elsevier.com/locate/inoche

Short communication

Effect of Cu^{2+} concentration on $MnFe_2O_4$ nano-crystals in its NH_3 sensing property

Deivatamil D.[a,d], John Abel Martin Mark[c], Sivaranjani S.[e], Thiruneelakandan Raghavan[b], Joseph Prince Jesuraj[c,*]

[a] Department of Physics, Periyar E.V.R. College, Tiruchirappalli 23, Tamil Nadu, India
[b] Department of Chemistry, University College of Engineering, Bharathidasan Institute of Technology Campus, Anna University, Tiruchirappalli 24, Tamil Nadu, India
[c] Department of Physics, University College of Engineering, Bharathidasan Institute of Technology Campus, Anna University, Tiruchirappalli 24, Tamil Nadu, India
[d] Manonmaniam Sundaranar University, Abishekapatti, Tirunelveli 627 012, Tamil Nadu, India
[e] Department of Physics, St.Antony's College of Arts and Sciences for Women, Ammakulathupatti, Tamil Nadu 624005, India

ARTICLE INFO

Keywords:
Co-precipitation route
Manganese ferrites
Gas sensor
Ammonia gas

ABSTRACT

This work is focused on the field of gas sensor for sensing the toxic gases which is highly harmful to environment. The semiconductor metal oxide nanoparticles of manganese ferrites and copper doped manganese ferrite ($MnFe_2O_4$ and Cu: $MnFe_2O_4$) was successfully developed. The characterization like crystal structure, surface morphology, optical bandgap, elemental composition and functional group analysis for the developed materials were carried out using X-ray Diffraction (XRD), Scanning electron microscope (SEM), Diffused reflectance spectroscopy (DRS), Energy dispersive X-Ray analysis (EDAX) and Fourier Transform (FT-IR) studies respectively. The ammonia gas (NH_3) was taken as test gas and the sensitivity of prepared samples were analyzed with different ppm (200–400) of gas molecules at room temperature. The sensing percentage gradually improved with the increase in Cu^{2+} concentration also with the increase in ppm of the gas. However, the recovery time of the material is increased with increase in the ppm.

1. Introduction

In recent decades, the scientific community has been showing much interest in manganese ferrites as gas-sensitive semiconductor materials, owing to their superior sensing property at all atmospheric conditions, high stability with durability cost-effectiveness, and facile fabrication process [1–7]. The basic mechanism of the gas sensors is, on exposing to different gas targets these semiconducting materials, can be sense the gas by the alteration of electrical conductivity with the chemi-absorbed vapor and/or interactivity with pre-adsorbed anions existing from the target gas. To synthesis semiconducting manganese ferrite nanopowders different types of chemical and physical methods have been employed [8–12]. The gas sensing properties can be influenced by the mode of preparation because the chemical and physical properties of the nanoparticles highly depend on the method employed. Therefore, understanding the growth parameters, such as pH and growth temperature, etc during the precipitation formation is of prime importance. Further, the resistivity of the nanopowders depends directly on the particle size; hypothetically in resistive type gas sensors particle size plays a vital role in the gas sensing property. The best way to decrease transient response of manganese ferrite semiconducting gas sensors is by decreasing the particle size of the nanopowders. In particular, a multi-functional semiconductor ferrite, such as, Manganese ferrite ($MnFe_2O_4$) is a fascinating semiconductor which has drawn considerable interest as a gas sensing material due to its salient micro-structural, morphological, chemical, thermal, and electrical properties [13–20].

The use of nanostructured $MnFe_2O_4$ for chemical sensors systems has a strong record which has been under comprehensive study among several other ferrite gas sensors, as it is seen in the literature, with the purpose to improve its gas sensing properties. $MnFe_2O_4$ has previously been demonstrated for its response to a variety of highly flammable and toxic fumes/vapors. In comparison, lesser attempts have been employed to detect reduction gases like, ammonia which is one of the gases that are toxic, colorless, and aromatic. Recent studies have focused on enhancing the sensitivity and response time of these gas sensors by either doping with sufficient dopant or changing the mechanism of synthesis. Although several techniques were developed for the preparation of nanoparticles [21–25] earlier, the conventional Co-

* Corresponding author.
E-mail address: josephprinceaut@gmail.com (J. Joseph Prince).

https://doi.org/10.1016/j.inoche.2021.108546
Received 17 December 2020; Received in revised form 26 February 2021; Accepted 26 February 2021
Available online 9 March 2021

precipitation method gets more attention in the preparation of nanopowders at relatively low temperature; by retaining its advantages. Similar to most of preparation techniques, this Co-precipitation method has its own process parameters and the optimization of grain size with adequate properties is predicted. In this paper, nanoparticles of $MnFe_2O_4$ and Cu^{2+} doped $MnFe_2O_4$ were prepared first and then coated over Stainless Steel (SS) substrate using doctor plate method for making gas sensors. The structural, morphological changes on the $MnFe_2O_4$ due to adding Cu^{2+} dopant and the gas sensing properties of $MnFe_2O_4$ and Cu^{2+} doped $MnFe_2O_4$ nanopowders are investigated.

2. Materials and methods:

2.1. Preparation of $MnFe_2O_4$ and Cu^{2+} doped $MnFe_2O_4$ powders

The nanoparticles of Manganese ferrites with the formula $Cu_{1-x}Mn_xFe_2O_4$ (x = 0, 1, 3 and 5 wt%) were developed by the facile chemical co-precipitation route. In this method, the constituents of the chemical precursors were metal nitrates such as $(Fe(NO_3)_3{\cdot}9H_2O)$ Iron (III) nitrate nonahydrate, $(Cu(NO_3)_2{\cdot}3H_2O)$ Copper (II) nitrate trihydrate and $(Mn(NO_3)_2{\cdot}4H_2O)$ Manganese (II) nitrate tetrahydrate and the solvent is Double Distilled (DD) water. Manganese and iron precursors are taken in 1: 2 ratios and dissolved in DD water, the precipitation agent used here is sodium hydroxide (NaOH) for preparing $MnFe_2O_4$ nanoparticles. The above procedure was repeated for making Cu doped $MnFe_2O_4$ nanoparticles by adding the copper precursor in appropriate amount and reducing the corresponding amount of manganese salt. The reaction was maintained with a pH of 11 by adding NaOH in consider quantity into the solution of metallic nitrates. Then, obtained slurry precipitate is centrifuge for several times and dried at 80 °C for 12 h. The obtained flakes of slurry were crushed into powder and the powder was air annealed at 700 °C for 4 h. The samples are denoted as MFO ($MnFe_2O_4$), CMF1 ($Cu_1Mn_{x-1}Fe_2O_4$), CMF2 ($Cu_3Mn_{x-3}Fe_2O_4$), and CMF3 ($Cu_5Mn_{x-5}Fe_2O_4$), in following sections.

2.2. Characterization techniques

XRD (Bruker D8 Advance) instrument used for examine the crystal structure of the nanopowders and the spectra was recorded in 2θ range from 15° to 80°. SEM instrument (Model: JSM-6701F) was utilized for morphological observation of the nanostructured materials. The optical absorption properties of the synthesized nanopowders were analyzed by using Shimadzu UV–Vis spectrophotometer between 300 and 800 nm. Jasco FTIR Spectrometer is used to analysis the various bonding present in the samples. The reducing gas sensing properties of manganese ferrites and nickel doped manganese ferrites were studied in a home-made gas sensor setup consisting of a 1.5 L volume gas chamber and furnace with temperature controller. The temperature control of the system was ranges from room temperature to 500 °C, and the resistance of the sensing materials in presence of relevant test fume ammonia and in air was measured using two-probe DC measurement technique. Ohmic contacts on the samples are made by conducting silver paste contact.

The gas response percentage is calculated as:

$$S(\%) = [(R_a - R_g)/Ra] \times 100 \quad (1)$$

where R_g material resistance in presence of gas and R_a is material resistance in air.

3. Results and discussion

3.1. Structural analysis

The structure and the phase purity of pure and copper doped $MnFe_2O_4$ were revealed by X-ray diffraction (XRD) analysis. The XRD patterns of doped $Mn_{1-x}Cu_xFe_2O_4$samples prepared at various Cu^{2+} concentrations (a (MFO), b (CMF1), c (CMF2), d (CMF3)) shown in Fig. 1. The observed peaks at 2θ = 30.2831, 35.5521, 43.2431, 53.5981, 57.0721, 62.7541 and 71.121 were indexed (JCPDS card No. 10-0319) [26] associated with planes (220), (311), (400), (422), (511), (440) and (533) respectively. After the indexing of diffraction patterns, it is evident that synthesized nanoparticles exhibited single phase cubic spinel structure. The addition of copper dopant to the manganese ferrite had not affected the crystal structure as well as no other secondary phase composites were formed in the process of making nanoparticles. In the XRD diffraction pattern the peak at 2θ = 35.5521 showed maximum intensity, which was from (311) Bragg planes. This peak has been considered for calculating the degree of crystallinity of the synthesized nanoparticles. To calculate the average crystallite size of Copper doped manganese ferrite samples Debye Scherrer formula was used.

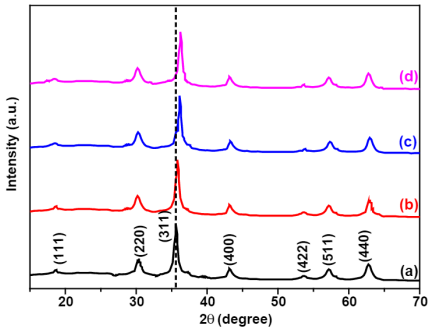

Fig. 1. XRD Diffraction of Copper doped Manganese Ferrite Nanoparticles.

Table 1
Crystallite Size and Lattice Parameter of the $MnFe_2O_4$ and Cu Doped $MnFe_2O_4$ nanoparticles using Debye Scherrer formula.

Materials	Lattice constant (Å)	Particle size, D (nm)
$MnFe_2O_4$	8.475	53.36
$Mn_{100\text{-}1\%}Cu_{1\%}Fe_2O_4$	8.467	48.35
$Mn_{100\text{-}3\%}\ Cu_{3\%}Fe_2O_4$	8.458	41.18
$Mn_{100\text{-}5\%}Cu_{5\%}Fe_2O_4$	8.454	36.35

$$D = 0.89\lambda/\beta\cos\theta \quad (2)$$

where λ the incident wavelength, D is the average crystallite size, β refers full width half maximum (FWHM), and θ refers angle of diffraction.

The copper dopant in $MnFe_2O_4$ retained the single-phase cubic structure of the nanoparticles but showed varying crystallite size in the synthesized nanoparticles. The average crystallite size calculated for MFO, CMF1, CMF2, and CMF3 samples ranging from 52.36 nm to 36.35 nm. The growth in crystallite size with the incorporation of Cu dopant revealed descending value from 52.36 nm to 36.35 nm with increasing Cu^{2+} concentration. But comparing the crystallite size of the pure $MnFe_2O_4$ with Cu doped $MnFe_2O_4$ nanoparticles it revealed that the higher values of Cu concentration resulted in decreasing value of crystallite size. This behavior is due the incorporation of Cu^{2+} with smaller ionic radii (0.73 Å) in the Mn^{2+} (0.82 Å) lattice sites during nucleation of grown nanoparticles Table 1.

3.2. Morphological studies

The Fig. 2(a, b, c, d) reveals the SEM photographs of undoped and Cu doped $MnFe_2O_4$ nanopowders. The surface of $MnFe_2O_4$ has no definite

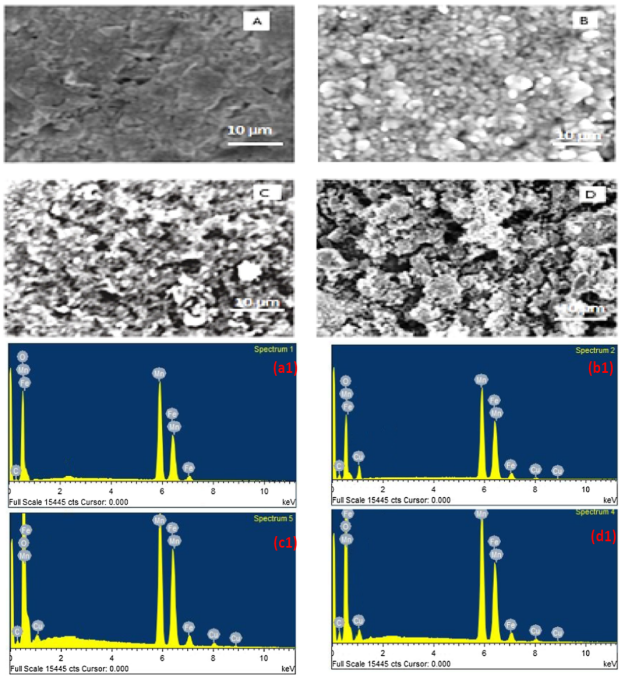

Fig. 2. (a, b, c, d) SEM images of Pure $MnFe_2O_4$, 1 wt%Cu: $MnFe_2O_4$, 3 wt%Cu: $MnFe_2O_4$ and 5 wt%Cu: $MnFe_2O_4$ respectively & (a1, b1, c1, d1) Respective EDAX spectrum.

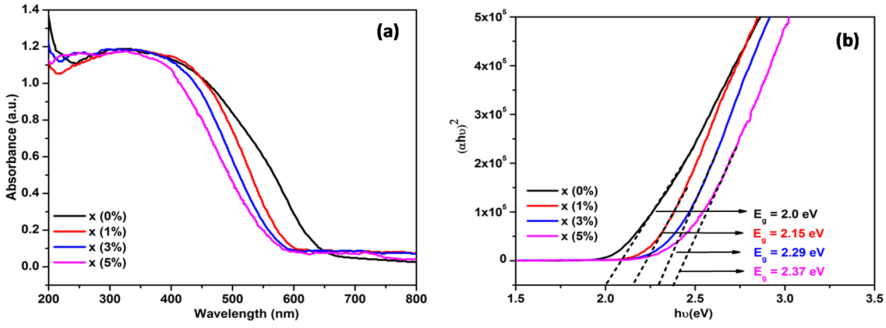

Fig. 3. (a) Absorbance spectra of undoped and Cu-doped $MnFe_2O_4$ nanopowders (b) Tauc's plot of Undoped and Cu doped $MnFe_2O_4$ nanopowders.

morphology and with smaller grains. Figure b represents the surface of 1 wt% Cu doped $MnFe_2O_4$, from no definite morphology (undoped $MnFe_2O_4$) to well defined spherical structure has been observed. The $MnFe_2O_4$with 3 wt% Cu doped sample manifest surface morphology, as it was expected with spherical particles which were shown in Fig. 2(c). Well defined sphere like surface morphology is obtained for 5 wt% Cu doped $MnFe_2O_4$ sample. Fig. 2(a1, b1, c1 & d1) shows the EDAX spectrum of MFO, CMF1, CMF2, and CMF3 respectively.

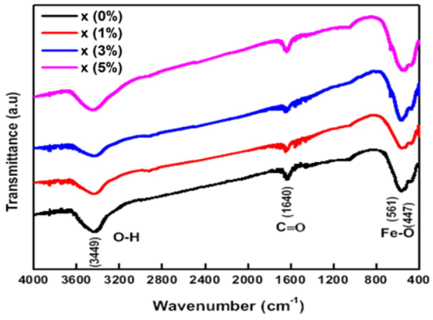

Fig. 4. FTIR spectrum of Cu doped $MnFe_2O_4$ nanopowders.

3.3. UV–Visible spectroscopy

Absorption spectra of the Cu doped $MnFe_2O_4$ nanopowders were prepared by pure and various dopant (Cu) concentrations of 1, 3 and 5 wt%. The spectra are recorded between 200 and 800 nm range and are illustrated in the Fig. 3(a). This figure demonstrating the dependence of wavelength and absorbance property for undoped $MnFe_2O_4$, and Cu doped $MnFe_2O_4$ for 1% Cu: $MnFe_2O_4$ and 3% Cu: $MnFe_2O_4$ and 5% Cu: $MnFe_2O_4$ respectively.

The optical band gap (E_g) of the developed materials were determined by using the Tauc's plot between hν and $(\alpha h\nu)^2$ which is the linear extrapolation of the absorption curve as represent in the Fig. 3(b). It is noted from the Tauc's plot as the Cu doping concentration increases the E_g value is also increases. In the case of the semiconductor like $MnFe_2O_4$, the coefficient of absorption α(ν) follows the corresponding spectral dependent absorption as a function of hν (photon energy) for direct band transitions, which can be derived from the Mott and Davis theory and is given below.

$$\alpha(\nu) = \frac{B(h\nu - Eg)^n}{h\nu} \tag{3}$$

Where n represents the character of the inter band transition of electrons, and B refers proportionality constant.

The optical band gap of the fabricated nano materials was measured using above relation. The band gap energy for pure $MnFe_2O_4$ is calculated to be 2.0 eV, which slightly increases to 2.15 eV for 1 wt% Cu: $MnFe_2O_4$, to 2.29 eV for 3 wt% Cu: $MnFe_2O_4$and to 2.37 eV for 5 wt% Cu: $MnFe_2O_4$, with a similar decrease in band gap been reported previously. The observed rise in the band gap may be attributed to the prelude of defects inside the band structure of the Cu^{2+} dopant ions. The fact is confirmed by the rise in the linear portion of the slope of the curve with the rising concentration of Cu^{2+} is found in the present work.

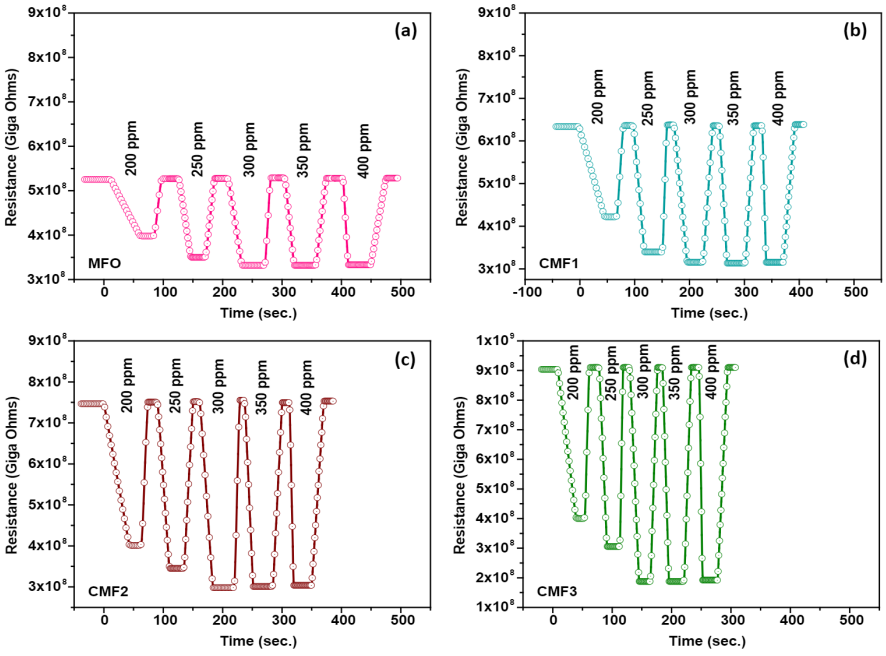

Fig. 5. Ammonia Sensitivity of pure and Cu doped $MnFe_2O_4$ nanopowder.

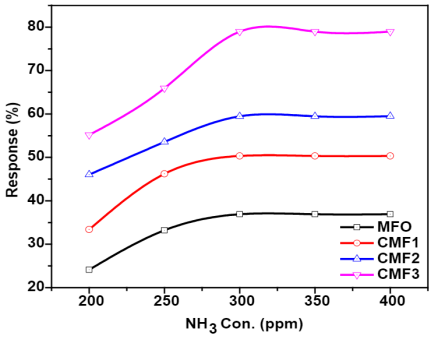

Fig. 6. Response percentages of prepared samples against different ppm of NH_3 gas.

3.4. FTIR studies

A significant technique used to detect the presence of metal–oxygen bands due to ion movements in the crystal lattice is FTIR spectroscopy. Fig. 4 shows the FTIR spectra of undoped and Cu doped $MnFe_2O_4$ nanopowders. For the powder samples, the transmission peaks in the range (581.7–639.6 cm^{-1}) and (462.1–576.7 cm^{-1}), are the two main metal–oxygen bands were observed which is corresponding to Mn-O and Fe-O vibrations at octahedral and tetrahedral sites, respectively, [27]. The shift in the location of the bands owing to Cu-doping can be related to the reduction in lattice constant values. Related findings were obtained with Co-doped $MnFe_2O_4$ nanoparticles. For all the samples, broader peaks emerged in the range (3441.2–3447.7 cm^{-1}), are corresponding to the stretching mode vibration of H-O-H bands of surface adsorbed water molecules present in the samples. [28]. In addition, the peaks observed at (1638.2–1640.1 cm^{-1}) range was related to the stretching mode of the C═O band.

3.5. Ammonia fumes sensing properties of the fabricated materials

The fumes sensitivity property of prepared nanopowder samples were examined using the home-made gas sensing set up. Fig. 5 (a, b, c, d) shows the relationship between change in resistance of the material for different ppm (200–400) of NH_3 gas response of pure and Cu doped $MnFe_2O_4$ nanoparticles. For every sample the sensitivity response towards ammonia improved with increase in ppm, and then saturated between 300 and 400 ppm. Sensitivity is the device feature of perceiving a difference in the sensing material's physical and/or chemical properties under exposure to gas. Using Eq. (1), the responsiveness of the nanoparticles that were coated as a film was determined. The maximum response percentage of 5 wt% Cu doped $MnFe_2O_4$ material is achieved to be 78% at moderate operating temperature (room temperature), which is the highest sensing response when compare to all the other prepared materials 3 wt% Cu: $MnFe_2O_4$(59%), 1 wt% Cu: $MnFe_2O_4$(50%) and

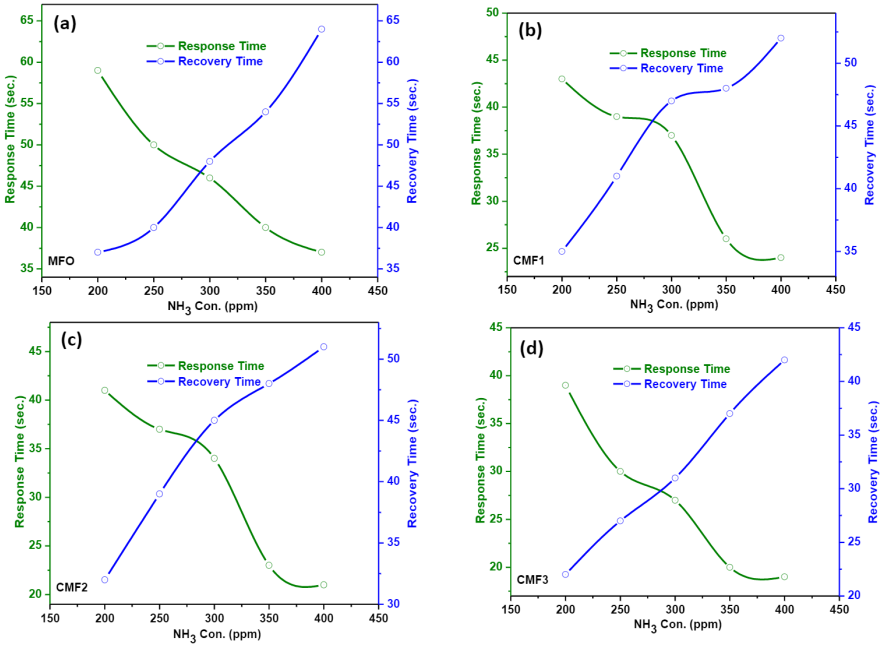

Fig. 7. Transient response characteristics of pure and Cu doped $MnFe_2O_4$ towards 200–400 ppm of ammonia at room temperature.

pure $MnFe_2O_4$ (36%) respectively. The response percentage corresponding to different ppm of NH_3 gas for all the samples is shown in Fig. 6. As the thermal energy of gas molecules not enough to make reaction with the O_2 species adsorbed on the surface at low temperatures, the sensing response of the material to NH_3 gas is limited due to the speed of the chemical reaction. In fact, a possible barrier to transport charges is formed during the adsorption of atmospheric oxygen to the surface of the film. Copper species would be uniformly distributed throughout the surface if the Cu^{2+} species are in sufficient amount and is incorporated in the surface of the $MnFe_2O_4$ material. Hence, the initial resistance of the material becomes low, and this property would effectively promote the catalytic reaction, so that the overall differences in the resistance of the material on the exposure of NH_3 gas give rise to an increase in the sensitivity. If the quantity of Cu^{2+} species on the material surface is less than the optimum value, the surface dispersion may be weak and the sensitivity of the material will decrease respectively.

3.6. Response and recovery times

The transient response characteristics of pure and Cu^{2+} doped $MnFe_2O_4$ films exposed to different ppm of ammonia at an operating temperature of 32 °C are shown in Fig. 7 (a, b, c, & d). In these experiments, different ppm of NH_3 gas was injected into the sealed glass tube and the resistivity of the sensors was measured with respect to time in the air and in the exposure of ammonia gas. From the figure it is clear that the sensing performance is gradually improved with the increasing concentration of Cu^{2+} on $MnFe_2O_4$, which is ascribed to a change in morphology and a remarkable decrease in the crystalline size of the doped samples, which considerably increase the oxygen absorption of the material. These oxygen adsorption increases the resistance of the sensor material owing to the electron transport from the conductive band to the adsorbed oxygen, and the electron is returned to the conductive band when this absorbed O_2 reacts with the test fume NH_3, leading to decreased in the resistance of the material. The 5 wt% Cu doped $MnFe_2O_4$ exhibited fast response and recovery time for ammonia gas. On the other hand it is noticed that all the samples shows fast responses but slow recovery at higher ppm of ammonia gas. The ammonia vapour highly reactive with adsorbed oxygen present in the Cu^{2+} sites on the sensor surface and also due to the high porous nature of the material, the faster response and recovery time for Copper doped manganese ferrites become possible. Fast and facile diffusion of gas into grain boundaries would allow the gas to be immediately oxidized, which in turn providing a rapid response.

4. Conclusion

Cu doped $MnFe_2O_4$ nanopowders were prepared using a chemical co-precipitation method. Cubic spinel structure formation was shown by XRD patterns of the samples, which showed variance in (311) peak intensities with Cu doping. The SEM analysis showed alteration of the surface morphology of $MnFe_2O_4$ due to Cu doping. Optical properties were strongly affected by the change in doping concentration. It is found that, the 5 wt% of Cu doped with $MnFe_2O_4$ showed an enhanced response to ammonia. The response and recovery times are good from 200 ppm of ammonia and are saturated between 300 and 400 ppm were observed for the sample with 5 wt% Cu doping at room temperature indicating promising material for ammonia detection.

Declaration of Competing Interest

The authors declare that they have no known competing financial interests or personal relationships that could have appeared to influence the work reported in this paper.

Acknowledgement

The authors wish to thank the staffs and all faculty members of department of Physics and Chemistry, UCE-BIT Anna University, Tiruchirappalli, for permitting to accesses all the facilities to carry out this study. The authors also like to give special thanks to the faculty members of Physic department Manonmaniam Sundaranar University, Tirunelveli for their assistance in characterization analysis.

References

[1] J. Kong, N.R. Franklin, C. Zhou, M.G. Chapline, S. Peng, K. Cho, H. Dai, Nanotube molecular wires as chemical sensors, Science 287 (2000) 622–625.
[2] J. Janata, M. Josowicz, P. Vanýsek, D.M. DeVaney, Chemical sensors, Anal. Chem. 70 (12) (1998) 179–208.
[3] P. Karthik, P. Gowthaman, M. Venkatachalam, M. Saroja, Design and fabrication of g-C_3N_4 nanosheets decorated TiO_2 hybrid sensor films for improved performance towards CO_2 gas, Inorg. Chem. Commun. 119 (2020) 108060, https://doi.org/10.1016/j.inoche.2020.108060.
[4] C.S. Jincy, P. Meena, Synthesis, Characterization, and NH3 Gas Sensing Application of Zn doped Cobalt Oxide Nanoparticles, Inorg. Chem. Commun. 120 (2020).
[5] S.D. Raut, V.V. Awasarmol, B.G. Ghule, S.F. Shaikh, S.K. Gore, R.P. Sharma, P. P. Pawar, R.S. Mane, Enhancement in room-temperature ammonia sensor activity of size-reduced cobalt ferrite nanoparticles on γ-irradiation, Mater. Res. Express 5 (6) (2018) 065035, https://doi.org/10.1088/2053-1591/aac99d.
[6] Z. Dong, X. Kong, Y. Wu, J. Zhang, Y. Chen, High-sensitive room-temperature NO_2 sensor based on a soluble n-type phthalocyanine semiconductor, Inorg. Chem. Commun. 77 (2017) 18–22.
[7] S. Kulkarni, P. Patil, A. Mujumdar, J. Naik, Synthesis and evaluation of gas sensing properties of PANI, PANI/SnO_2 and PANI/SnO_2/rGO nanocomposites at room temperature, Inorg. Chem. Commun. 96 (2018) 90–96.
[8] Y. Shimizu, S. Kai, Y. Takao, T. Hyodo, M. Egashira, Correlation between methyl mercaptan gas-sensing properties and its surface chemistry of SnO2-based sensor materials, Sens. Actuators B Chem. 65 (2000) 349–357.
[9] X.-J. Huang, Y.-K. Choi, Chemical sensors based on nanostructured materials, Sens. Actuators B Chem. 122 (2) (2007) 659–671.
[10] A. Kolmakov, Y. Zhang, G. Cheng, M. Moskovits, Detection of CO and O_2 using tin oxide nanowire sensors, Adv. Mater. 15 (12) (2003) 997–1000.
[11] J.-H. Lee, Gas sensors using hierarchical and hollow oxide nanostructures: overview, Sens. Actuators B Chem. 140 (1) (2009) 319–336.
[12] X. Lai, G. Shen, P. Xue, B. Yan, H. Wang, P. Li, W. Xia, J. Fang, Ordered mesoporous NiO with thin pore walls and its enhanced sensing performance for formaldehyde, Nanoscale 7 (9) (2015) 4005–4012.
[13] A.A. Bagade, V.V. Ganbavle, S.V. Mohite, T.D. Dongale, B.B. Sinha, K.Y. Rajpure, Assessment of structural, morphological, magnetic and gas sensing properties of $CoFe_2O_4$ thin films, J. Colloid Interface Sci. 497 (2017) 181–192.
[14] R.H. Vignesh, K.V. Sankar, S. Amaresh, Y.S. Lee, R.K. Selvan, Synthesis and characterization of $MnFe_2O_4$ nanoparticles for impedometric ammonia gas sensor, Sens. Actuators B Chem. 220 (2015) 50–58.
[15] L. Li, J. Tan, M. Dun, X. Huang, Porous ZnFe2O4 nanorods with net-worked nanostructure for highly sensor response and fast response acetone gas sensor, Sens. Actuators B Chem. 248 (2017) 85–91.
[16] K. Subbiah, L. Han-Seung, L. Yun Su, S. Jitendra Kumar, K. Seung-Jun, N. Rethinam, Fabrication of a cerium-doped nickel ferrite solid-state reference electrode and its performance evaluation in concrete environment, Sens. Actuators B Chem. 251 (2017) 509–523.
[17] Y. Zhang, Y.u. Zhou, Z. Li, G. Chen, Y. Mao, H. Guan, C. Dong, MOFs-derived $NiFe_2O_4$ fusi form is with highly selective response to xylene, J. Alloys Compd. 784 (2019) 102–110.
[18] A.F.S. Abu-Hani, S.T. Mahmoud, F. Awwad, A.I. Ayesh, Design, fabrication, and characterization of portable gas sensors based on spinel ferrite nanoparticles embedded in organic membranes, Sens. Actuators B Chem. 241 (2017) 1179–1187.
[19] Y.u. Yuan, B. Wang, C. Wang, X. Li, J. Huang, H. Zhang, F. Xia, J. Xiao, Effects of $CoFe_2O_4$ electrode microstructure on the sensing properties for mixed potential NH_3 sensor, Sens. Actuators B Chem. 239 (2017) 462–466.
[20] S. Zhuiykov, T. Ono, N. Yamazoe, N. Miura, High-temperature NOx sensors using zirconia solid electrolyte and zinc-family oxide sensing electrode, Solid State Ion. 152–153 (2002) 801–807.
[21] L.M. Thorat, J.Y. Patil, D.Y. Nadargi, R.C. Kambale, S.S. Suryavanshi, Ni^{2+} substituted Mg-Cu-Zn ferrites by molten salt route: Evaluation of structural, morphological and electromagnetic properties, Inorg. Chem. Commun. 99 (2019) 20–25.
[22] X. Zhang, H. Sun, S. Tan, J. Gao, Y. Fu, Z. Liu, Hydrothermal synthesis of Ag nanoparticles on the nano-cellulose and their antibacterial study, Inorg. Chem. Commun. 100 (2019) 44–50.
[23] G.K. Weldegebrieal, Synthesis method, antibacterial and photocatalytic activity of ZnO nanoparticles for azo dyes in wastewater treatment: a review, Inorg. Chem. Commun. 120 (2020), 108140.
[24] B.N. Rashmi, S.F. Harlapur, B. Avinash, C.R. Ravikumar, H.P. Nagaswarupa, M.R. A. Kumar, M.S. Santosh, Facile green synthesis of silver oxide nanoparticles and their electrochemical, photocatalytic and biological studies, Inorg. Chem. Commun. 111 (2019), 107580.

[25] H.R. Saadati-Moshtaghin, F.M. Zonoz, In situ preparation of CeO_2 nanoparticles on the MCM-41 with magnetic core as a novel and efficient catalyst for the synthesis of substituted pyran derivatives, Inorg. Chem. Commun. 99 (2019) 44–51.
[26] B. Sahoo, S.K. Sahu, S. Nayak, D. Dhara, P. Pramanik, Fabrication of magnetic mesoporous manganese ferrite nanocomposites as efficient catalyst for degradation of dye pollutants, Catal. Sci. Technol. 2 (2012) 1367–1374.
[27] W.B. Carpenter, J.A. Fournier, R. Biswas, G.A. Voth, A. Tokmakoff, Delocalization and stretch-bend mixing of the HOH bend in liquid water, J. Chem. Phys. 147 (2017), 084503.
[28] M.H. Habibi, H.J. Parhizkar, FTIR and UV–vis diffuse reflectance spectroscopy studies of the wet chemical (WC) route synthesized nano-structure $CoFe_2O_4$ from $CoCl_2$ and $FeCl_3$, Spectrochim. Acta A Mol. Biomol. Spectrosc. 127 (2014) 102–106.